Acta Crystallographica Section D
Biological Crystallography
ISSN 0907-4449

Structures of three diphtheria toxin repressor (DtxR) variants with decreased repressor activity

Ehmke Pohl,[a,b]*† Joanne Goranson-Siekierke,[c] Michael K. Choi,[c] Tarmo Roosild,[d]‡ Randall K. Holmes[c] and Wim G. J. Hol[a,b,d,e]

[a]Department of Biological Structure, University of Washington, Seattle, WA 98195, USA, [b]Department of Biochemistry, University of Washington, Seattle, WA 98195, USA, [c]Department of Microbiology, University of Colorado Health Sciences Center, Denver, CO 80262, USA, [d]Biomolecular Structure and Design Program, University of Washington, Seattle, WA 98195, USA, and [e]Howard Hughes Medical Institute, University of Washington, Seattle, WA 98195, USA

† Current address: European Molecular Biology Laboratory, Hamburg Outstation, Notkestrasse 85, 22603 Hamburg, Germany.
‡ Current address: Salk Institute, San Diego, California 92186-5800, USA.

Correspondence e-mail: ehmke@embl-hamburg.de

Received 30 October 2000
Accepted 1 February 2001

PDB References: Cys102Ser-DxR-I, 1g3s; Cys102Ser-DtxR-II, 1g3t; Cd-Cys102Ser-DtxR, 1g3w; Zn-Arg80Ala-DtxR, 1g3y; Zn-Glu20Ala-DtxR, 1fwz.

The diphtheria toxin repressor (DtxR) from *Corynebacterium diphtheriae* regulates the expression of the gene on corynebacteriophages that encodes diphtheria toxin (DT). Other genes regulated by DtxR include those that encode proteins involved in siderophore-mediated iron uptake. DtxR requires activation by divalent metals and holo-DtxR is a dimeric regulator with two distinct metal-binding sites per three-domain monomer. At site 1, three side chains and a sulfate or phosphate anion are involved in metal coordination. In the DtxR–DNA complex this anion is replaced by the side chain of Glu170 provided by the third domain of the repressor. At site 2 the metal ion is coordinated exclusively by constituents of the polypeptide chain. In this paper, five crystal structures of three DtxR variants focusing on residues Glu20, Arg80 and Cys102 are reported. The resolution of these structures ranges from 2.3 to 2.8 Å. The side chain of Glu20 provided by the DNA-binding domain forms a salt bridge to Arg80, which in turn interacts with the anion. Replacing either of the salt-bridge partners with an alanine reduces repressor activity substantially and it has been inferred that the salt bridge could possibly control the wedge angle between the DNA-binding domain and the dimerization domain, thereby modulating repressor activity. Cys102 is a key residue of metal site 2 and its substitution into a serine abolishes repressor activity. The crystal structures of Zn-Glu20Ala-DtxR, Zn-Arg80Ala-DtxR, Cd-Cys102Ser-DtxR and apo-Cys102Ser-DtxR in two related space groups reveal that none of these substitutions leads to dramatic rearrangements of the DtxR fold. However, the five crystal structures presented here show significant local changes and a considerable degree of flexibility of the DNA-binding domain with respect to the dimerization domain. Furthermore, all five structures deviate significantly from the structure in the DtxR–DNA complex with respect to overall domain orientation. These results confirm the importance of the hinge motion for repressor activity. Since the third domain has often been invisible in previous crystal structures of DtxR, it is also noteworthy that the SH3-like domain could be traced in four of the five crystal structures.

1. Introduction

Toxigenic strains of the human pathogen *C. diphtheriae* produce diphtheria toxin (DT), which causes severe damage in various tissues of the body (Barksdale, 1970). The structural gene for DT is encoded by bacteriophages such as phage β and DT expression is regulated at the transcriptional level by iron (Pappenheimer, 1977) and the diphtheria toxin repressor

Table 1
Crystallographic data and refinement statistics.

	C102S-I	C102S-II	Cd-C102S	Zn-R80A	Zn-E20A
Unit-cell parameters					
$a = b$, c (Å)	63.6, 110.3	63.0, 216.0	63.5, 110.0	62.8, 109.2	63.7, 106.9
α, β, γ (°)	90, 90, 120	90, 90, 120	90, 90, 120	90, 90, 120	90, 90, 120
Space group	$P3_121$	$P3_221$	$P3_121$	$P3_121$	$P3_121$
Temperature (K)	293	100	293	100	100
Resolution (Å)	2.4	2.35	2.5	2.8	2.3
Unique reflections	10070	19654	8957	6373	11094
Completeness (%)	94.5	90.5	94.1	98.0	95.3
$R_{\rm merge}$† (%)	0.061	0.053	0.050	0.078	0.084
Protein residues	4–140, 148–197, 201–225	3–140, 148–198, 201–226, 3–140	4–140, 148–197, 201–224	3–140, 148–156, 159–198, 201–225	4–140, 148–198, 201–223
Water	79	138	74	24	139
R factor (%)	0.185	0.238	0.180	0.224	0.196
$R_{\rm free}$	0.271	0.318	0.259	0.328	0.285
B, metal 1	—	—	41	20	28
$\lvert B\rvert$‡ (Å^2)	51	39	53	27	49
R.m.s.d.s					
Bond lengths	0.009	0.009	0.010	0.008	0.013
Angles	1.7	1.5	1.6	1.5	1.8

† $R_{\rm merge} = \sum |I - \langle I\rangle| / \sum I$. ‡ Average B factor for non-H atoms, protein only.

(DtxR) (Boyd *et al.*, 1990; Schmitt *et al.*, 1992). Under high-iron conditions, DtxR acts as a negative regulator by binding its target DNA sequence in regulated promoters and preventing transcription of the downstream genes (Boyd *et al.*, 1990; Schmitt *et al.*, 1992; Tao *et al.*, 1994; Holmes, 2000). DtxR controls not only the expression of DT but also of a heme oxygenase (Schmitt, 1997) and several components of the iron-uptake and the oxidative-stress systems (Schmitt & Holmes, 1994; Schmitt *et al.*, 1997; Lee *et al.*, 1997). Whereas *in vivo* only Fe^{2+} activates the repressor, *in vitro* several other divalent transition metals including Zn^{2+}, Ni^{2+}, Mn^{2+}, Co^{2+} and Cd^{2+} have been shown to activate DtxR (Schmitt *et al.*, 1992; Tao *et al.*, 1992; Tao & Murphy, 1992).

In recent years, DtxR homologues have been identified in a number of bacteria, including *Streptomyces* (Günther-Seeboth & Schupp, 1995), *Brevibacterium lactofermentum* (Oguiza *et al.*, 1996), *Mycobacterium* (Schmitt *et al.*, 1995; Doukhan *et al.*, 1995), *Treponema pallidum* (Hardham *et al.*, 1997), *Staphylococcus* (Hill *et al.*, 1998) and *Rhodococcus* (Boland & Meijer, 2000). Evidently, the important human pathogens that cause tuberculosis, leprosy, syphilis and staphylococcal infections all possess homologues of DtxR. Therefore, the biological function of gene regulation by the DtxR family in pathogens is of great interest and has been studied in some detail. The mycobacterial homologue, also designated IdeR (iron-dependent regulator), has been shown to negatively regulate siderophore synthesis *in vivo* (Schmitt *et al.*, 1995; Dussurget *et al.*, 1996, 1999). Furthermore, Manabe *et al.* (1999) demonstrated that a constitutively active DtxR variant attenuates the virulence of *M. tuberculosis in vivo*. These results clearly indicate that repressors of the DtxR/IdeR family may play an important role in regulating virulence-associated genes in pathogenic bacteria (Dussurget & Smith, 1998).

In order to further elucidate the activation mechanism of this family of regulators, crystal structures of DtxR in complex with different divalent transition metals have been studied in depth (Qiu *et al.*, 1995, 1996; Schiering *et al.*, 1995; Pohl *et al.*, 1997, 1998). These structures revealed an N-terminal DNA-binding domain (residues 1–73) that contains the familiar helix–turn–helix DNA-binding motif. The second, dimerization domain (residues 74–140) provides most of the ligands of the two metal-binding sites: (i) the side chains of His79, Glu83 and His98 at metal site 1 and (ii) the side chains of residues Glu105, His106, Cys102 and the carbonyl O atom of Cys102 at site 2. The coordination of the metal at site 1 is completed by an anion whose protein ligands are Arg80, Ser126 and Asn130 (Qiu *et al.*, 1996). Site 2 showed lower occupancy than site 1 in the first wt-DtxR structures, but was later confirmed to be present with high occupancy in the crystal structures of the Cys102Asp-DtxR variant (Ding *et al.*, 1996) and of *M. tuberculosis* IdeR (Pohl *et al.*, 1999*a*; Feese, Ingason *et al.*, 2001). In both crystal structures, the side chain of residue Met10 from the DNA-binding domain completes the coordination of site 2. The flexible third domain, consisting of residues 148–226, adopts an SH3-like fold (Qiu *et al.*, 1996; Wang *et al.*, 1999). A detailed comparison of the apo- and holo-repressor showed a movement of the DNA-binding domain with respect to the dimerization domain as a possible activation mechanism (Pohl *et al.*, 1998). This hinge motion was later confirmed both in the crystal structure of the Cys102Asp-DtxR variant in complex with DNA (White *et al.*, 1998; Chen *et al.*, 2000) and of the wild-type DtxR–DNA complex (Pohl *et al.*, 1999*b*). In addition, the latter structure demonstrated for the first time an interaction of the third domain with the metal-binding site 1 as well as with the anion-binding residues. These results provided the first evidence that the anion-binding residues are involved in the activation mechanism (reviewed by Feese, Pohl *et al.*, 2001).

Saturation site-directed mutagenesis studies indicated that Cys102 is essential for the activation of DtxR. Replacement of this residue by any other amino acid except aspartic acid resulted in loss of regulatory activity (Tao & Murphy, 1993). Subsequent random and site-directed mutagenesis studies based on the first crystal structure of DtxR (Qiu *et al.*, 1995, 1996) showed that residues involved in metal binding as well as in anion binding at site 1 are important for DtxR function (Wang *et al.*, 1994; Goranson-Siekierke *et al.*, 1999). Single alanine substitutions of anion-binding residues resulted in a loss of repressor activity nearly comparable to site 2 substitutions (Goranson-Siekierke *et al.*, 1999). Here, we report the

crystal structures of three single-site variants of DtxR that exhibit markedly decreased repressor activity: Cys102Ser, Arg80Ala and Glu20Ala. The Cys102Ser-DtxR variant was chosen to probe the metal binding at site 2. We have determined the crystal structures of the Cys102Ser mutant in the apo form in two related space groups as well as in complex with Cd^{2+}. In the wild-type DtxR structure, Arg80 has a dual role. First, this side chain serves as one ligand to the anion at metal-binding site 1 and second, it forms an important ionic interaction with Glu20, thus establishing a link from the metal site 1 to the DNA-binding domain. Substituting either Arg80 or Glu20 with alanine caused a dramatic decrease in repressor activity (Goranson-Siekierke *et al.*, 1999). In order to illuminate the role of the Arg80 and Glu20 residues, we determined the crystal structures of the two single-site variants, Arg80Ala-DtxR and Glu20Ala-DtxR, both in complex with Zn^{2+}.

2. Experimental section

2.1. Protein expression, purification and crystallization

The cloning and overexpression of the three DtxR variants in *Escherichia coli* has been described previously (Schmitt *et al.*, 1992; Goranson-Siekierke *et al.*, 1999). Briefly, all proteins were overexpressed in *E. coli* and purified using a Ni-NTA affinity column followed by anion-exchange chromatography (Schmitt & Holmes, 1993). The Arg80Ala-DtxR and Glu20Ala-DtxR variants were further purified by hydroxyapatite chromatography. The overexpression and purification was verified by SDS–PAGE and by mass-spectrometric analysis (data not shown). All variants were crystallized by hanging-drop vapor diffusion at room temperature. For all crystallization experiments the proteins were kept in a buffer of 10 m*M* Tris pH 8.0, 100 m*M* NaCl. The protein concentration of the Cys102Ser-DtxR variant was 3.6 mg ml^{-1}. The reservoir solution contained 100 m*M* Tris buffer pH 8.5, 1.85 *M* ammonium sulfate. Diffracting crystals were obtained when 5% glycerol was added to the reservoir solution before mixing the drops in a 3:2 ratio of protein and reservoir solution. The Cd-Cys102Ser-DtxR crystals were obtained from the same solution with 1 m*M* Cd^{2+} in the reservoir and the metal-free crystals with 1 m*M* EDTA in the reservoir. The protein concentration of the Glu20Ala-DtxR and Arg80Ala-DtxR variants was 2.2 mg ml^{-1}. These variants were crystallized by mixing 6 µl protein solution and 2 µl reservoir solution containing 100 m*M* Tris buffer pH 8.5, 2.0 *M* ammonium sulfate and 5% glycerol. Suitable crystals were only obtained with 10 m*M* Zn^{2+} in the reservoir solution. In all three cases, trigonal shaped crystals with dimensions up to 0.4 × 0.4 × 0.3 mm appeared after 1–4 weeks. The crystals were isomorphous to wild-type DtxR crystals with the same two space groups $P3_121$ or $P3_221$ as described previously (Pohl *et al.*, 1998).

2.2. Data collections and processing

The apo-Cys102Ser-DtxR (form I) and Cd-Cys102Ser-DtxR crystals were mounted in a capillary and data were collected at room temperature. No significant radiation decay was observed. In the three other cases, the crystals were flash-cooled in a rayon loop using the reservoir solution with 15–25% glycerol as a cryoprotectant (Teng, 1990). Diffraction data were collected on an R-AXIS II imaging-plate detector using monochromatic Cu $K\alpha$ radiation and focusing mirrors. The data were integrated and processed with *DENZO* and *SCALEPACK* (Otwinowski & Minor, 1997). Integrated intensities were converted into structure factors using *TRUNCATE* (French & Wilson, 1978).

2.3. Structure solution and refinement

The coordinates of residues 6–140 of Co-wt-DtxR at 1.85 Å resolution (Pohl *et al.*, 1997) were used as a search model for molecular replacement using *AMoRe* (Navaza, 1994). In all cases 5% of the data were used to calculate the free *R* values (Brünger, 1992, 1993). The models were completed by iterative cycles of simulated annealing and conjugate-gradient least-squares refinement with the program *X-PLOR* (Brünger *et al.*, 1987). The σ_A-weighted (Read, 1986) $2F_o - F_c$ and $F_o - F_c$ electron-density maps were inspected and the model was completed using the interactive graphics program *O* (Jones *et al.*, 1991). The final round of refinement included coordinates and restrained individual *B*-factor refinement. Further crystallographic key data are summarized in Table 1.

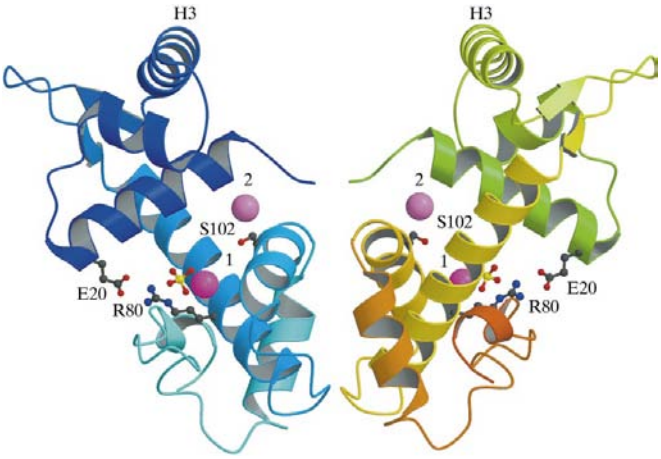

Figure 1
Ribbon representation of the Cd-Cys102Ser-DtxR dimer in crystal form I. The view shown is approximately perpendicular to the crystallographic twofold axis. One monomer is shown with the colors changing from the N-terminal DNA-binding domain in dark blue to the dimerization domain in light blue. The second monomer is presented with the colors changing from the N-terminal DNA-binding domain in green to the dimerization domain through yellow to orange. The third domain has been omitted for clarity of the picture. The three amino-acid substitution sites Glu20, Arg80 and Ser102 and the sulfates are indicated in ball-and-stick representation. The metal-binding site 1 present in all holo-structures is shown as a magenta sphere and the metal-binding site 2 is shown in purple (the coordinates were taken from the Mn-wt-DtxR structure of Qiu *et al.*, 1996). All figures were prepared using *Molscript* (Kraulis, 1991), its extended version *Bobscript* (Esnouf, 1997) and/or *Raster3d* (Merritt & Bacon, 1997).

3. Results

3.1. Quality of the models

All three DtxR variants were crystallized in the same trigonal space group $P3_121$, with one monomer per asymmetric unit (crystal form I). In each case the crystallographic models include the DNA-binding domain (residues 1–74), the dimerization domain (residue 75–140) and the flexible SH3-like third domain (residues 148–226). In addition, the three holo-structures contain a cadmium (Cys102Ser-DtxR) or zinc cation (Arg80Ala-DtxR and Glu20Ala-DtxR) as a cofactor. For the Zn-Glu20Ala-DtxR variant there is also one sulfate anion close to metal site 1. In the Cd-Cys102Ser-DtxR structure the anion at site 1 appeared to be only partially occupied. In all four crystal form I structures the first two or three N-terminal and the last C-terminal residues and two linker regions (residues 141–147 and 198–200) were not traceable in the electron-density maps and were therefore not included in the crystallographic models (see Table 1). In addition, a number of polar side-chain atoms in the flexible third domain showed no density and were thus refined as alanines. In the Arg80Ala-DtxR structure only metal-binding site 1 is occupied by a Zn atom. Presumably owing to the lower resolution of 2.8 Å, a loop region in the third domain (residues 156–159) was also invisible in the electron density and was omitted from the refinement. In the case of apo-Cys102Ser-DtxR, the second crystal form reported for the wt-DtxR crystal structures (Pohl *et al.*, 1998) was also obtained. In this crystal form II, the crystallographic twofold symmetry is replaced by a non-crystallographic twofold axis. Hence, the *c* axis of the unit cell is doubled, the space group changes from $P3_121$ to $P3_221$ and the asymmetric unit contains one dimer with a non-crystallographic twofold symmetry. Here, the first two domains were found to be well ordered, but the third domain was traceable only in the first monomer and was completely invisible in the second monomer. This domain and the disordered linkers (residue 141–147 and 198–200) were not included in the final model. The same phenomenon has been described for various wt-DtxR structures (Pohl *et al.*, 1998).

In all five crystal structures described here, the substituted residues were not included in the initial refinement steps and the initial unbiased σ_A-weighted $F_o - F_c$ electron-density maps (Read, 1986) unambiguously identified the alanine or serine residues at the position of the substitution. The final models possessed good geometry for bond lengths and angles, with all residues in the allowed regions of the Ramachandran plot (data not shown).

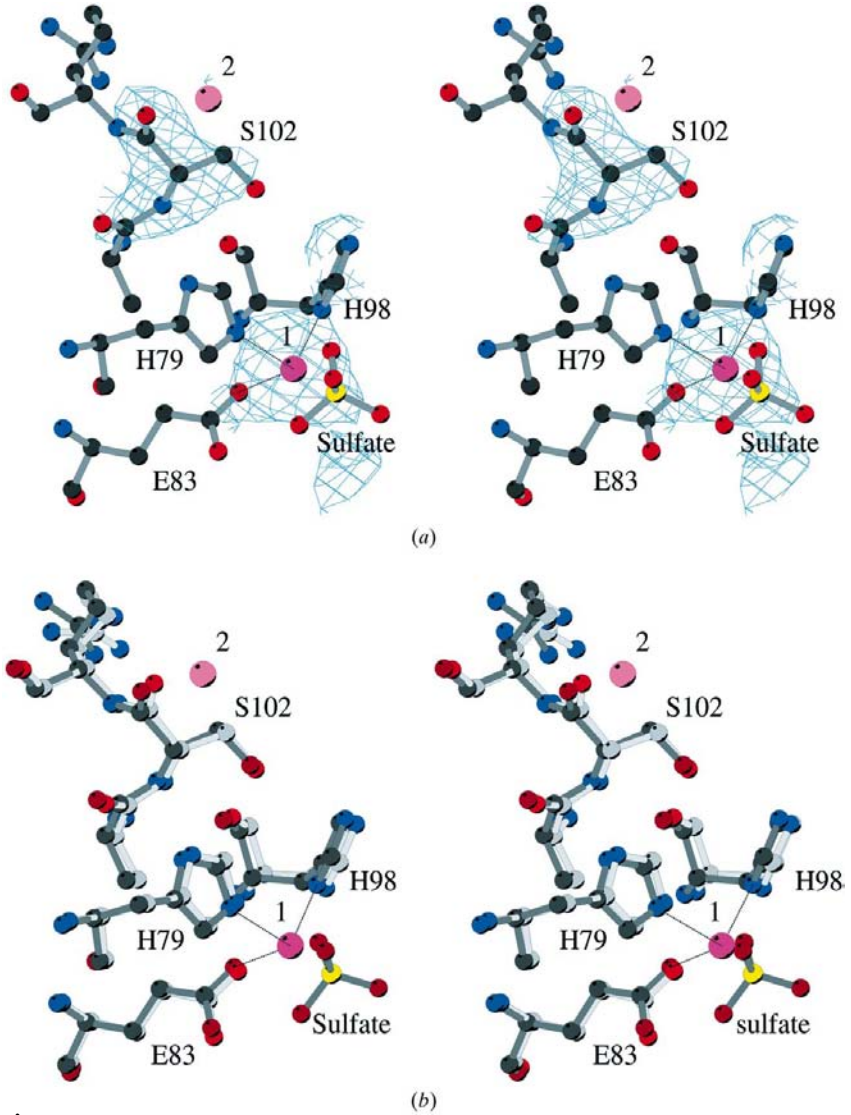

Figure 2
Stereoview of the metal-binding site 1 of the Cd-Cys102Ser-DtxR structure in crystal form I at 2.5 Å (*a*) showing the unbiased σ_A-weighted $F_o - F_c$ electron-density maps (Read, 1986) at a 1.3σ level, (*b*) showing the comparison of the Cd-Cys102Ser-DtxR (dark grey bonds) with apo-Cys102Ser-DtxR (open bonds) at 2.5 Å resolution after least-squares superposition of the first two domains. The second metal-binding site taken from the Mn-wt-DtxR structure (Qiu *et al.*, 1996) is indicated in purple.

3.2. General description of the structures

The crystal structure of the Cd-Cys102Ser-DtxR dimer in crystal form I at 2.5 Å resolution is depicted in Fig. 1. The view shown is approximately perpendicular to the crystallographic twofold axis and along the DNA-binding helices H3. In this figure, the two amino acids Glu20 and Arg80, which are replaced by Ala in the two other mutants described here, residue Ser102, the sulfate anion and the metal sites are shown in ball-and-stick representations. Metal-binding site 1 is fully occupied in all holo-DtxR variants presented in this paper, whereas site 2 is not occupied. The position shown in Fig. 1 has been taken from the Mn-wt-DtxR structure

Table 2
R.m.s. deviations (in Å) for least-squares superposition of DtxR structures in crystal form I.

The superposition was calculated for the 135 common C^{α} atoms of the first two domains (residues 6–140).

	Mn-DtxR†	Apo-C102S	Cd-C102S	Zn-R80A	Zn-E20A
Apo-wtDtxR‡	0.56	0.56	0.74	0.31	0.29
Mn-wtDtxR		0.36	0.50	0.63	0.61
Apo-C102S			0.26	0.49	0.53
Cd-C102S				0.60	0.62
Zn-R80A					0.36

† Qiu *et al.* (1996). ‡ Pohl *et al.* (1998).

(Qiu *et al.*, 1996). The overall fold of the protein is conserved upon mutation and not drastically altered in any of the five structures. The r.m.s. deviations for the least-squares superposition of 135 common C^{α} atoms of domains 1 and 2 of the three DtxR variants and apo-wt-DtxR are in the range 0.29–0.74 Å (see Table 2). The local changes associated with each amino-acid substitution will be discussed in more detail in the following sections.

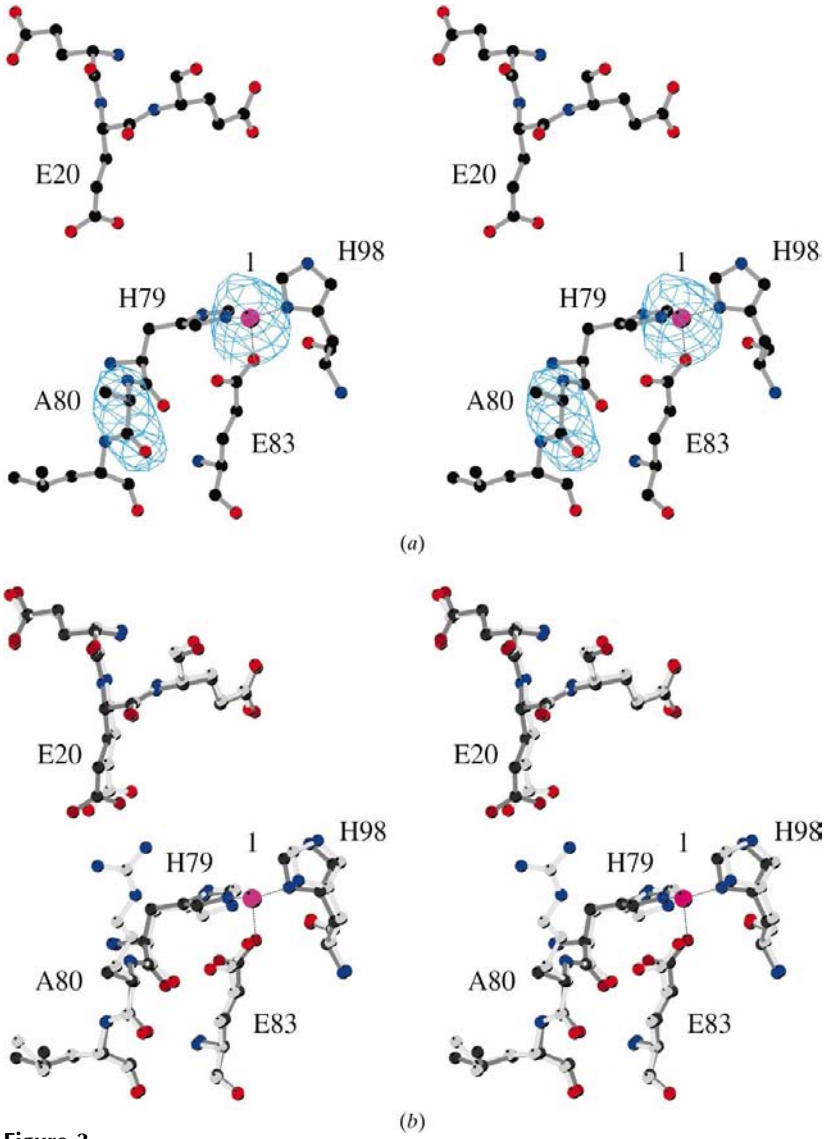

Figure 3
Stereoview of the metal-binding site 1 of the Zn-Arg80Ala-DtxR structure at 2.8 Å (*a*) showing the unbiased σ_A-weighted $F_o - F_c$ electron-density maps (Read, 1986) at the 2σ level and (*b*) presenting the comparison of Zn-Arg80Ala-DtxR (dark grey bonds) with apo-wt-DtxR (open bonds) at 2.3 Å resolution (Pohl *et al.*, 1998) after least-squares superposition of the first two domains.

3.3. Cys102Ser-DtxR

The apo-Cys102Ser-DtxR variant was crystallized in two related space groups as described above. The holo-structure was crystallized with Cd^{2+} as a cofactor in crystal form I only. The initial unbiased electron density clearly showed the substitution site as well as metal site 1 (Fig. 2*a*). The highest peak in the difference electron density of 23σ was found here; however, the neighboring sulfate displayed only weak density. Therefore, the sulfate was later refined assuming an occupancy of 0.5. It is important to note that in contrast to the Cd-wt-DtxR structure (Qiu *et al.*, 1995), the metal-binding site 2 (indicated in violet in Fig. 2) is not occupied; no significant electron density above 3σ was found near this site in the difference electron-density map. The comparison between the two apo-Cys102Ser-DtxR structures and the Cd-Cys102Ser-DtxR structures reveals no changes in the overall fold. The r.m.s. deviation for 135 C^{α} atoms of the first two domains is only 0.26 Å. The least-squares superposition of the Cd-Cys102Ser-DtxR variant with the apo-Cys102Ser-DtxR structure depicted in Fig. 2(*b*) shows no significant alteration upon metal binding. The small deviations visible in Fig. 2(*b*) are within the accuracy of the crystal structure determination. The superposition of the Cys102Ser-DtxR variant monomers with apo- and holo-wt-DtxR again shows only small conformational changes (data not shown). The r.m.s. deviations for the 135 C^{α} atoms of the first two domains are between 0.29 and 0.74 Å (see also Table 2). The hinge motion between the DNA-binding and the second domain for all three DtxR variants will be discussed further below.

3.4. Arg80Ala-DtxR

The Arg80Ala-DtxR variant could only be crystallized with zinc as a cofactor in crystal form I. The initial electron-density map unambiguously revealed the mutation as well as the presence of a metal at site 1 (Fig. 3*a*). The highest maximum (9.1σ) in the unbiased $F_o - F_c$ difference density was found at metal site 1. The second metal-binding site was found to be empty, presumably owing to partial oxidation of Cys102 as described for the wild-type DtxR structures (Qiu *et al.*, 1996; Pohl *et*

al., 1997). It is noteworthy that there is no significant electron density above 3σ for the anion or any other metal ligand near site 1. The comparison of Zn-Arg80Ala-DtxR with the holo-wt-DtxR structure shows no apparent changes arising from the substitution, despite the fact that the Arg80–Glu20 salt bridge is obviously no longer present in the mutant. The overall structures of mutant and wild-type repressors are very similar, with r.m.s. deviations of 0.31–0.61 Å for 135 C^{α} atoms of the first two domains. All the side-chain conformations are essentially the same as in the wild-type DtxR structure (Fig. 3*b*). The position of Glu20 which acts as the salt-bridge partner in the wild-type structure remains almost unchanged. Even the side-chain *B* factors of the side-chain atoms of Glu20 are only slightly increased (average B = 46.7 Å^2) compared with the Cys102Ser-DtxR structure (average B = 40.7 Å^2).

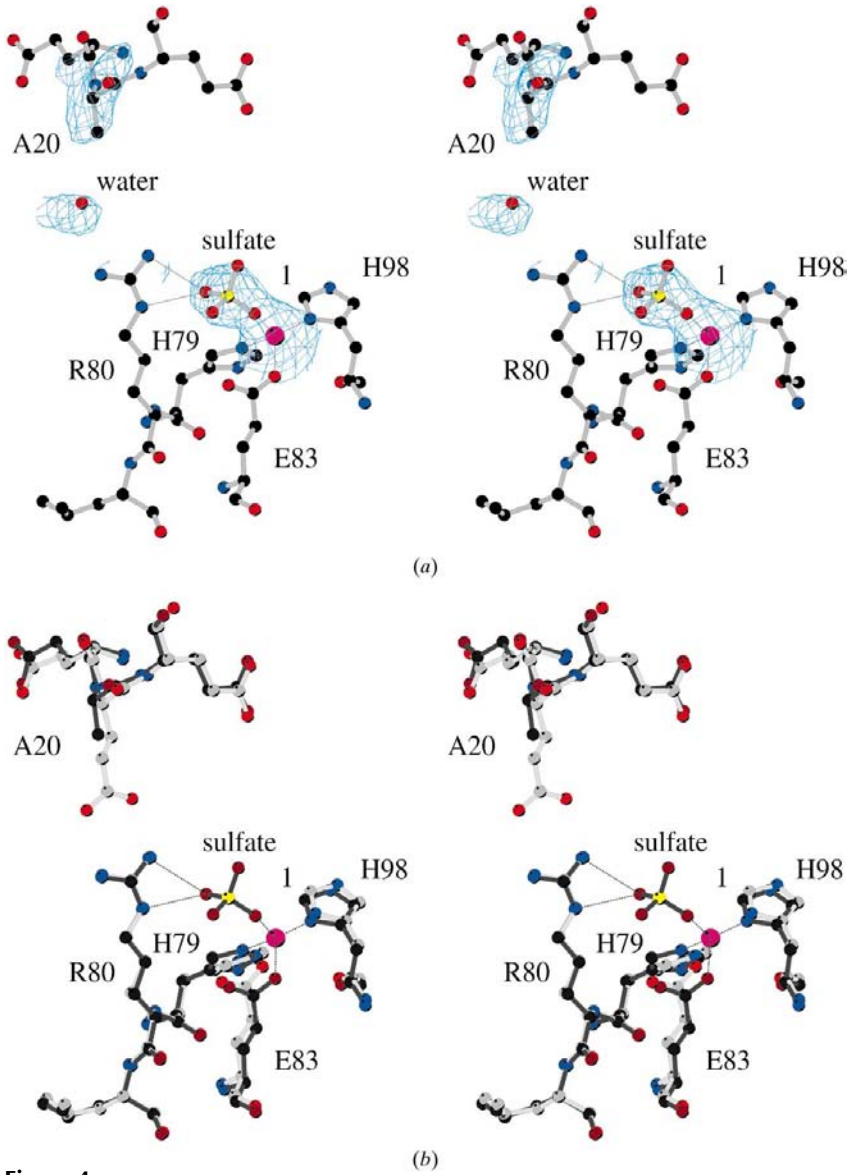

Figure 4
Stereoview of the metal-binding site 1 of the Zn-Glu20Ala-DtxR structure at 2.3 Å (*a*) showing the unbiased σ_A-weighted $F_o - F_c$ electron-density maps (Read, 1986) at the 2σ level and (*b*) showing the comparison of the Zn-Glu20-Ala-DtxR (dark grey bonds) with apo-wt-DtxR (open bonds) (Pohl *et al.*, 1998) after least-squares superposition of the first two domains.

3.5. Glu20Ala-DtxR

The Glu20Ala-DtxR variant was also crystallized with zinc as cofactor in crystal form I. As for the previous DtxR variants, the initial electron density clearly revealed the correct amino acid at the substitution site as well as the metal at binding site 1. Here, the maximum of the unbiased difference electron density of 14.3σ was located at site 1, whereas the second highest peak of 7.1σ was identified at the anion-binding site (Fig. 4*a*). In this case, the height and shape of the density clearly reveals the sulfate anion as the fourth ligand of the metal. After including the zinc cation, the sulfate anion and the third domain in the refinement, the highest peak in the difference electron-density map was found close to the S^{γ} of Cys102. The density revealed a similar oxidation or modification as described previously for the wild-type DtxR structures (Qiu *et al.*, 1996; Pohl *et al.*, 1997). As in the case of the Arg80Ala variant and despite the loss of the Arg80–Glu20 salt bridge, the Glu20Ala-DtxR structure remains very similar to the wild-type DtxR structure. The r.m.s. deviation of the 135 C^{α} atoms of the first two domains of Glu20Ala-DtxR and wt-DtxR is between 0.29 and 0.61 Å. All residues of metal-binding site 1 superimpose nearly perfectly (Fig. 4*b*). A water molecule in the variant fills the space of the Glu20 side chain in the wild-type DtxR structure, while the position of Arg80 is maintained (Fig. 4*a*). The side-chain *B* factors of this residue (average B = 20.5 Å^2) are almost identical to the *B* factors of the Cd-Cys102Ser variant (average B = 20.4 Å^2).

3.6. Domain motion of DtxR

In order to analyze the presence of a hinge motion between the DNA-binding and the dimerization domain, we compared the tertiary structure of all DtxR variants presented in this paper with the following structures: (i) apo-wt-DtxR (crystal forms I and II) (Pohl *et al.*, 1998; PDB codes 1bi1, 1bi2), (ii) Mn-wt-DtxR as an example for a holo-DtxR structure (Qiu *et al.*, 1996) and (iii) Co-wt-DtxR bound to DNA (Pohl *et al.*, 1999*b*; PDB code 1cow). To address a possible motion of the dimerization domains, the 67 common C^{α} atoms (residues 74–140) in one monomer were superimposed and the transformation was applied to the full dimer. The results of this operation show that this domain remains very similar in all structures, with r.m.s. deviations between 0.21 and 0.88 Å (Table 3). After applying this transformation to the full dimer, the r.m.s. deviations for the second dimerization domain

Table 3
R.m.s. deviations (in Å) for the superposition of the dimerization domains of DtxR dimers.

The lower left part of the table gives the r.m.s. deviation of the 67 C^{α} atoms of the dimerization domain in the first subunit. The upper right part summarizes the resulting r.m.s. deviations of the dimerization domain in the second subunit after superpositioning the first dimerization domain.

	Apo-wt-DtxR, form I†	Apo-wt-DtxR, form II†	Mn-DtxR‡	Apo-C102S, form I	Apo-C102S, form II	Cd-C102S	Zn-R80A	Zn-E20A	Co-wt-DtxR-DNA§
Apo-wDtxR-I		0.50	0.93	1.31	0.61	1.29	0.43	0.55	0.85
Apo-wt-DtxR-II	0.15		1.24	0.87	0.22	0.82	0.31	0.51	0.77
Mn-DtxR	0.64	0.64		1.21	1.32	1.04	1.15	1.14	1.25
Apo-C102S-I	0.63	0.54	0.25		0.90	0.69	0.90	1.24	1.36
Apo-C102S-II	0.21	0.22	0.67	0.61		0.83	0.32	0.55	0.80
Cd-C102S	0.88	0.70	0.44	0.25	0.76		0.81	1.05	1.08
Zn-R80A	0.23	0.27	0.62	0.61	0.26	0.75		0.53	0.71
Zn-E20A	0.18	0.22	0.64	0.61	0.21	0.75	0.22		0.45
Co-wt-DtxR-DNA	0.41	0.43	0.60	0.60	0.47	0.68	0.42	0.38	

† Pohl *et al.* (1998). ‡ Qiu *et al.* (1996). § Pohl *et al.* (1999*b*).

Table 4
R.m.s. deviations (in Å) for the superposition of DNA-binding domains.

The lower left part of the table gives the r.m.s. deviation of all 68 C^{α} atoms of the DNA-binding domain in the first subunit. The upper right part summarizes the resulting r.m.s. deviations of the 68 C^{α} atoms of the DNA-binding domain in the second subunit after superimposing the first DNA-binding domain.

	Apo-wt-DtxR, form I†	Apo-wt-DtxR, form II†	Mn-DtxR‡	Apo-C102S, form I	Apo-C102S, form II	Cd-C102S	Zn-R80A	Zn-E20A	Co-wt-DtxR-DNA§
Apo-wt-txR-I		0.60	1.03	1.06	0.66	1.22	0.44	1.26	2.79
Apo-wt-DtxR-II	0.21		0.95	1.02	0.38	1.27	0.99	1.32	3.12
Mn-DtxR	0.28	0.29		0.90	0.98	1.80	1.29	2.18	3.66
Apo-C102S-I	0.26	0.34	0.24		1.07	1.13	1.41	1.95	3.78
Apo-C102S-II	0.22	0.27	0.30	0.33		1.09	0.77	1.17	3.02
Cd-C102S	0.26	0.36	0.30	0.22	0.34		0.92	1.46	2.91
Zn-R80A	0.31	0.31	0.41	0.29	0.29	0.29		0.76	2.62
Zn-E20A	0.26	0.32	0.36	0.30	0.37	0.27	0.28		2.15
Co-wt-DtxR-DNA	0.37	0.51	0.44	0.40	0.44	0.42	0.43	0.50	

† Pohl *et al.* (1998). ‡ Qiu *et al.* (1996). § Pohl *et al.* (1999*b*).

which was not used to calculate the superposition matrix are only slightly higher, with values between 0.32 and 1.36 Å. These results show that the dimerization domains do not change their relative orientation in the crystal structures used in this comparison.

For the analysis of a motion of the DNA-binding domains, the 68 common C^{α} atoms (residues 7–74) in one monomer were first superimposed and the transformation was then applied to the full DtxR dimer. The results of this operation are summarized in Table 4. In all cases, the first DNA-binding domains by themselves superimpose very well, with r.m.s. deviations between 0.21 and 0.51 Å for all possible combinations. Thus, the conformation of the DNA-binding domain remains essentially the same in all structures independent of whether or not the co-repressor and/or DNA are bound. However, after the DNA-binding domains of the first subunit of two dimers are superimposed, the DNA-binding domains of the second subunit that have not been used to calculate the transformation matrix show a significant motion. The r.m.s. deviations range from 0.44 to 2.18 Å among the DtxR structures not bound to DNA (Table 4). Among these, the largest difference is observed when comparing our new Zn-Glu20Ala-DtxR structure with Mn-wt-DtxR (Qiu *et al.*, 1996). This structure possesses a partially occupied metal-binding site II. Significantly larger motions of the second DNA-binding domain with respect to the first DNA-binding domain are observed when the Co-wt-DtxR-DNA structure (Pohl *et al.*, 1999*b*) is taken into account. The largest overall motion is observed between the new apo-Cys102Ser-DtxR (crystal form I) and wt-DtxR in the Co-wt-DtxR-DNA (r.m.s. difference for the second DNA-binding domain is 3.8 Å). This domain motion is clearly evident for all other DtxR variants used in our comparison (Fig. 5).

4. Conclusions

Although the repressor activity is severely decreased in the three new DtxR variants described here, the comparison of their structures with wild-type DtxR shows no significant changes in the overall fold. On a more detailed level, there are small but important changes arising from the amino-acid substitutions. In contrast to the Cd-wt-DtxR structure, where the Cd^{2+} was found to be present, albeit not with full occupancy, at metal-binding site 2 (Qiu *et al.*, 1995), this site is clearly empty in the Cd-Cys102Ser-DtxR variant. The O atom of the Ser102 side chain is apparently energetically less favorable for metal binding than the S atom of the cysteine side chain, so that the presence of the three unchanged ligands at this site, Glu105, His106 and the carbonyl of Ser102, are not sufficient for metal binding. Hence, site 2 is empty and the regulator shows decreased activity. This result is consistent with the previous findings of the mutational analysis that only the native Cys102 or an Asp102 substitution is sufficient for proper functioning of the repressor (Tao & Murphy, 1993; Ding *et al.*, 1996). At position 102 only the S^{γ} of the cysteine side chain or the O^{δ} of an aspartate can function as a ligand for metal-binding site 2.

The crystal structures of the Arg80Ala-DtxR and Glu20Ala-DtxR variants show that the removal of the salt bridge between the side chains of Arg80 and Glu20 in the wild-type repressor does not result in a noticeably different structure from wt-DtxR. Even the side-chain conformation of the second residue remains almost unchanged upon removal

of the partner of the salt bridge. In the wt-DtxR structure these two residues form a link between the DNA-binding domain and the metal-binding domain (Qiu *et al.*, 1995). In addition, the side chain of Arg80 interacts *via* two guanidinium H atoms with the anion (Qiu *et al.*, 1996). In the Zn-Arg80Ala-DtxR structure described here, the anion-binding site is empty although the metal-binding site 1 is clearly fully occupied. It appears that the interaction with the Arg80 side chain is necessary for anion binding. In the wt-DtxR-DNA complex (Pohl *et al.*, 1999*b*) the side chain of Arg80 is within hydrogen-bonding distance of the side chain of Glu170 of the third domain, which in turn coordinates the metal. Thus, Arg80 may play a role in positioning the third domain with respect to the two other domains and thereby affect the properties of the regulator. The absence of the Arg80 side chain may prevent the third domain from obtaining its optimal position for DNA binding.

The exact role of the Glu20 side chain has yet to be elucidated. Substitution of this side chain does not change the conformation of any side chain significantly, including that of its salt-bridge partner Arg80. It might be possible that crystal packing prevents the observation of the full spectrum of conformations available to the Glu20Ala-DtxR mutant in solution. In other words, in the mutants without the salt bridge the ensemble of structures in solution may have a larger variation of hinge angles than in the case of wt-DtxR. The Glu20–Arg80 salt bridge may function by stabilizing the protein in solution in the conformation that is capable of DNA binding. Intervening with the metal–Glu170–Arg80–Glu20 chain of interactions by removing the side chain of either Glu20 or Arg80 may increase the flexibility of the DNA-binding domain with respect to the second domain. Further studies are obviously required to investigate this possibility.

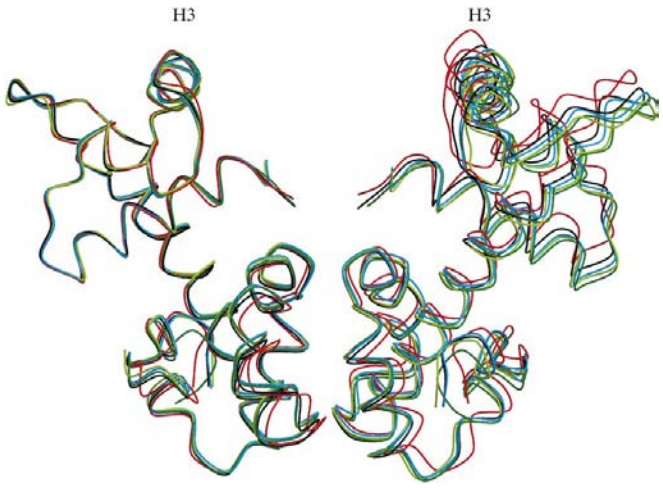

Figure 5
Least-squares superposition of DtxR variants with wt-DtxR bound to DNA. Only the DNA-binding domain from monomer *A* on the left side was used to calculate the transformation matrix that was then applied to the full dimer. The apo-Cys102Ser-DtxR structure is shown in light green, Cd-Cys102Ser-DtxR in green, Zn-Glu20Ala-DtxR in blue, Zn-Arg80Ala-DtxR in black and wt-DtxR bound to DNA (Pohl *et al.*, 1999*b*) in red.

In the five crystal structures of three DtxR variants presented here, there are remarkable differences in the mutual orientation of the DNA-binding domains in the dimer. The conformations observed in these crystal structures show again a hinge motion of the DNA-binding domain that repositions the two DNA-binding helices in each dimer with respect to each other. The non-activated form of DtxR can therefore be described as adopting multiple states where the conformation observed in the crystal depends on the degree of metal binding as well as on crystal packing. The fully activated form of DtxR as observed in the Co-wt-DtxR-DNA structure undergoes a considerably larger motion that changes the position of equivalent C^{α} atoms of the second DNA-binding domain up to an r.m.s. deviation of 3.8 Å. Evidently, a hinge motion of the DNA-binding domain with respect to the dimerization domain is an intrinsic property in the DtxR family of iron-dependent repressors and is critical for its functioning.

This work was supported by the NIH grant R01CA65656 to WGJH and NIH grant R01AI4107 to RKH, by a major equipment grant from the Murdock Charitable Trust to the Biomolecular Structure Center, by the NRSA grant to JGS and by an Ernst-Schering Research Foundation postdoctoral fellowship to EP. We would like to thank S. Turley for his help during data collection and maintaining the in-house area detectors.

References

Barksdale, L. (1970). *Bacteriol. Rev.* **34**, 378–422.
Boland, C. A. & Meijer, W. G. (2000). *FEMS Microbiol. Lett.* **191**, 1–5.
Boyd, J., Oza, M. & Murphy, J. R. (1990). *Proc. Natl Acad. Sci. USA*, **87**, 5968–5972.
Brünger, A. T. (1992). *Nature (London)*, **355**, 472–474.
Brünger, A. T. (1993). *Acta Cryst.* D**49**, 24–36.
Brünger, A. T., Kuriyan, J. & Karplus, M. (1987). *Science*, **235**, 458–460.
Chen, C. S., White, A., Love, J., Murphy, J. R. & Ringe, D. (2000). *Biochemistry*, **39**, 10397–10407.
Ding, X., Zeng, H., Schiering, N., Ringe, D. & Murphy, J. R. (1996). *Nature Struct. Biol.* **3**, 382–387.
Doukhan, L., Predich, M., Nair, G., Dussurget, O., Mandic Mulec, I., Cole, S. T., Smith, D. R. & Smith, I. (1995). *Gene*, **165**, 67–70.
Dussurget, O., Rodriguez, M. & Smith, I. (1996). *Mol. Microbiol.* **22**, 535–544.
Dussurget, O. & Smith, I. (1998). *Trends Microbiol.* **6**, 354–358.
Dussurget, O., Timm, J., Gomez, M., Gold, B., Yu, S., Sabol, S. Z., Holmes, R. K., Jacobs, W. R. Jr & Smith, I. (1999). *J. Bacteriol.* **181**, 3402–3408.
Esnouf, R. M. (1997). *J. Mol. Graph.* **15**, 133–138.
Feese, M. D., Ingason, M. P., Goranson-Siekierke, J., Holmes, R. K. & Hol, W. G. J. (2001). *J. Biol. Chem.* **276**, 5959–5966.
Feese, M. D., Pohl, E., Holmes, R. K. & Hol, W. G. J. (2001). *Handbook of Metalloproteins*, edited by K. Wieghardt, R. Huber, T. L. Poulos & A. Messerschmidt. Chichester: John Wiley & Sons.
French, G. S. & Wilson, K. S. (1978). *Acta Cryst.* A**34**, 517–525.
Goranson-Siekierke, J., Pohl, E., Hol, W. G. J. & Holmes, R. K. (1999). *Infect. Immun.* **67**, 1806–1811.
Günther-Seeboth, K. & Schupp, T. (1995). *Gene*, **166**, 117–119.

Hardham, J. M., Stamm, L. V., Porcella, S. F., Frye, J. G., Barnes, N. Y., Howell, J. K., Mueller, S. L., Radolf, J. D., Weinstock, G. M. & Norris, S. J. (1997). *Gene*, **197**, 47–64.
Hill, P. J., Cockayne, A., Landers, P., Morrissey, J. A., Sims, C. M. & Williams, P. (1998). *Infect. Immun.* **66**, 4123–4129.
Holmes, R. K. (2000). *J. Infect. Dis.* **181**, S156–S167.
Jones, T. A., Zou, J. Y., Cowan, S. W. & Kjeldgaard, M. (1991). *Acta Cryst.* A**47**, 110–119.
Kraulis, P. (1991). *J. Appl. Cryst.* **24**, 946–950.
Lee, J. H., Wang, T., Ault, K., Liu, J., Schmitt, M. P. & Holmes, R. K. (1997). *Infect. Immun.* **65**, 4273–4280.
Manabe, Y. C., Saviola, B. J., Sun, L., Murphy, J. R. & Bishai, W. R. (1999). *Proc. Natl Acad. Sci. USA*, **96**, 12844–12848.
Merritt, E. A. & Bacon, D. J. (1997). *Methods Enzymol.* **277**, 505–525.
Navaza, J. (1994). *Acta Cryst.* A**50**, 157–163.
Oguiza, J. A., Marcos, A. T., Malumbres, M. & Martin, J. F. (1996). *J. Bacteriol.* **178**, 550–553.
Otwinowski, Z. & Minor, W. (1997). *Methods Enzymol.* **276**, 307–326.
Pappenheimer, A. M. (1977). *Annun. Rev. Biochem.* **46**, 69–94.
Pohl, E., Holmes, R. K. & Hol, W. G. J. (1998). *J. Biol. Chem.* **35**, 22420–22427.
Pohl, E., Holmes, R. K. & Hol, W. G. J. (1999*a*). *J. Mol. Biol.* **292**, 653–667.
Pohl, E., Holmes, R. K. & Hol, W. G. J. (1999*b*). *J. Mol. Biol.* **285**, 1145–1156.
Pohl, E., Qiu, X., Must, L., Holmes, R. K. & Hol, W. G. J. (1997). *Protein Sci.* **6**, 1114–1118.
Qiu, X., Pohl, E., Holmes, R. K. & Hol, W. G. J. (1996). *Biochemistry*, **35**, 12292–12302.
Qiu, X., Verlinde, C. J. L. M., Zhang, Z., Schmitt, M. P., Holmes, R. K. & Hol, W. G. J. (1995). *Structure*, **3**, 87–100.
Read, R. J. (1986). *Acta Cryst.* A**42**, 140–149.
Schiering, N., Tao, X., Zeng, H., Murphy, J. R., Petsko, G. A. & Ringe, D. (1995). *Proc. Natl Acad. Sci. USA*, **92**, 9843–9850.
Schmitt, M. P. (1997). *Infect. Immun.* **65**, 4634–4641.
Schmitt, M. P. & Holmes, R. K. (1993). *Mol. Microbiol.* **9**, 173–181.
Schmitt, M. P. & Holmes, R. K. (1994). *J. Bacteriol.* **176**, 1141–1149.
Schmitt, M. P., Predich, M., Doukhan, L., Smith, I. & Holmes, R. K. (1995). *Infect. Immun.* **63**, 4284–4289.
Schmitt, M. P., Talley, B. G. & Holmes, R. K. (1997). *Infect. Immun.* **65**, 5364–5367.
Schmitt, M. P., Twiddy, E. M. & Holmes, R. K. (1992). *Proc. Natl Acad. Sci. USA*, **89**, 7576–7580.
Tao, X., Boyd, J. & Murphy, J. R. (1992). *Proc. Natl Acad. Sci. USA*, **89**, 5897–5901.
Tao, X. & Murphy, J. R. (1992). *J. Biol. Chem.* **267**, 21761–21764.
Tao, X. & Murphy, J. R. (1993). *Proc. Natl Acad. Sci. USA*, **90**, 8524–8528.
Tao, X., Schiering, N., Zeng, H., Ringe, D. & Murphy, J. R. (1994). *Mol. Microbiol.* **14**, 191–197.
Teng, T. Y. (1990). *J. Appl. Cryst.* **23**, 387–391.
Wang, Z., Schmitt, M. P. & Holmes, R. K. (1994). *Infect. Immun.* **62**, 1600–1608.
Wang, G., Wylie, G. P., Twigg, P. D., Caspar, D. L., Murphy, J. R. & Logan, T. M. (1999). *Proc. Natl Acad. Sci. USA*, **96**, 6119–6124.
White, A., Ding, X., vanderSpek, J. C., Murphy, J. R. & Ringe, D. (1998). *Nature (London)*, **394**, 502–506.